Acta Oceanologica Sinica 2006, Vol. 25, No. 2, p. 1~24
http://www.oceanpress.com.cn
E-mail: hyxbe@263.net

Fronts and strong currents of the upper southeast Indian Ocean

HE Zhigang[1,2], DONG Zhaoqian[2*], YUAN Xiaojun

1. Department of Oceanography, Xiamen University, Xiamen 361005, China
2. Polar Research Institute of China, Shanghai 200136, China
3. Lamont-Doherty Earth Observatory, Columbia University, Palisades, New York NY 10964-800, USA

Received 18 October 2005; accepted 7 January 2006

Abstract

Hydrographic data, ADCP velocity and sea level anomaly derived from the satellite altimeter have been jointly analyzed in the southeast Indian Ocean. Results show the locations and orientations of the major oceanic fronts as well as the characteristics of the currents within these fronts in the area. Double subtropical fronts are observed in the section along 120°E, which conflicts with the frontal structure frequently observed before–the North Subtropical Front (NSTF) and South Subtropical Front (SSTF) merge into a single STF between 110°~115°E. The Subantarctic Front (SAF), influenced by the out-of-phase double eddies, runs across 48°S three times between 120° and 127°E. The surface current within the SAF is strengthened up to 105.4 cm/s by the geostrophic effect of these eddies. Furthermore eddies may cause the strong current to split up into two branches within the SAF. The SAF and the primary polar front (PF1) can be identified individually in the ADCP data with a separation distance of about 0.3° at latitude between 140° and 145°E, although they cannot be identified separately in the low-resolution hydrographic data. The different thermohaline characteristics of Circumpolar Deep Water (CDW) and Modified Circumpolar Deep Water (MCDW) result in the formation of Southern Antarctic Circumpolar Current Front (SACCF) in the southeast Indian Ocean. It consistently turns northward along the east flank of the Kerguelen Plateau after it runs through the Princess Elizabeth Trough and turns southward sharply north of 60°S with a little seasonal variations. It is shown that the locations and orientations of the SAF, the primary PF and SACCF in the ACC of the southeast Indian Ocean can be identified more precisely by the current distribution derived from ADCP data than by hydrographic data, because these fronts are usually accompanied by strong currents. However, the locations and orientations of the STF and the secondary PF are more difficult to be identified through current data, since these two fronts are usually not accompanied by any jet. The STF the and the secondary PF are usually confined in the first few hundred meters of the upper ocean and the latter is often determined by the northern terminus of 2 ℃ isothermal.

Key words: southeast Indian Ocean, front, jet

1 Introduction

Baroclinic component is the dominant part of Antarctic Circumpolar Current (ACC) (Fandry and Pillsbury, 1979), and a baroclinic transportation associated with fronts makes up the majority part of the total baroclinic transportation of the ACC (Nowlin and Clifford, 1982). Therefore the strong currents within the ACC in the southeast Indian Ocean must be closely related to the oceanic fronts.

Although the observations in the southeast Indian Ocean are relatively rare, many scholars depicted the characteristics and variations of fronts in the southeast Indian Ocean using inadequate in situ observations and remote sensing data. Belkin and Gordon.(1996, BG96 hereafter) used less than 200 quasi-meridional sections to investigate the main fronts between 0° and 150° E and found that there were typical tri-front structure in the southeast Indian Ocean. The three fronts are the

* Corresponding author, E-mail: dongzhaoqian@pric.gov.cn

Subtropical Front (STF), Subantarctic Front (SAF) and Polar Front (PF). The newly defined North Subtropical Front (NSTF) and the South Subtropical Front (SSTF) (usually defined as the STF) merge into a single STF between 110° and 115°E. The SAF extends eastward along the north flank of the Southeast Indian Ridge, while the PF extends eastward along the south flank (refer to Fig. 4 in BG96). Orsi et al. (1995, OWN95 hereafter) showed the approximate paths of the STF, SAF, PF and the Southern Antarctic Circumpolar Current Front (SACCF) in the Southern Ocean utilizing historical hydrographic data from 32 meridional sections, in which seven sections were in the southeast Indian Ocean. In addition to the conventional analysis, Sun and Watts (2002) also examined the variation of PF and SAF with a streamfuntion projection from historical data. They found that the PF position varies little in the streamfunction space, but the SAF exhibits a significant meridional deflection. Compared with the in situ observations, remote sensing data have the advantages of high spatial and temporal resolution, good synchronism and longer time series. On the basis of the 7 a satellite-derived sea surface temperature, Moore et al.(1999) studied the location and dynamics of the PF. They found that the mean path of PF is strongly steered by the topographic features of the Southern Ocean. The topography places vorticity constraints on the dynamics of PF and consequently affects spatial and temporal variabilities of the front.

The locations of fronts derived from hydrographic data obtained from the Chinese National Antarctic Research Expeditions (CHINARE) cruises and international corporations have been studied by Chinese scholars and the main results are shown in Fig.1 (Su and Dong, 1984; Miao et al., 1995; Shi et al., 1995; Gao et al., 1995; Gao et al., 2003; Pu et al., 2002; Yuan et al., 2004). Yuan et al. (2004) defined the northern terminus of 2 ℃ isotherm at the temperature minimum layer as the secondary PF, which is different from the PF definition of BG96. They also defined the strong lateral thermal gradient extending deep in the water column between the SAF and the secondary PF as the primary PF. Su and Dong (1984) defined this feature as the mean location of the polar front zone. However, the primary and secondary polar fronts may not be clearly separated in some historical observations. The locations and paths of the SAF and the secondary PF derived by Chinese scholars (Su and Dong, 1984; Miao et al., 1995; Shi et al., 1995; Gao et al., 1995; Yuan et al., 2004) agree well with those of BG96. It is difficult to show an approximate path of the STF due to the uneven distribution of the inadequately detected STF locations (see Fig. 1).

Except for the STF, SAF and PF in the ACC, there exists another circumpolar front—the Southern ACC Front (SACCF) south of the PF, which was found and termed by OWN95. It is the only front in the ACC that does not separate distinct surface water masses. The northern limit of the front coincides with the potential temperature less than 0 ℃ along the temperature minimum layer at depth less than 150 m. The southern limit is where potential temperature is greater than 1.8 ℃ at the depth greater than 500 m or where the salinity is greater than 34.73 at the depth deeper than 800 m. It can be summarized from the results of in situ observations and models that the SACCF in the southern Indian Ocean turns southward between 30° and 40°E, and then eastward right north of the continent slope of Antarctica, passes through the Princess Elizabeth Trough at about 63°S, and turns north along the east flank of the Kerguelen Plateau. It reaches its northern limit between 55° and 60°S east of the Kerguelen Plateau and then turns southeastward (OWN95; Sparrow et al., 1996; Heywood et al., 1999; Shi et al., 2002).

Although many scientists have investigated the oceanic fronts in the southern Indian Ocean, most of studies were based on thermohaline properties of the fronts. Because of limited observations, the current structures associated with those fronts were rarely examined. We believe that the baroclinitic transport dominants the total ACC transport and intense baroclinic

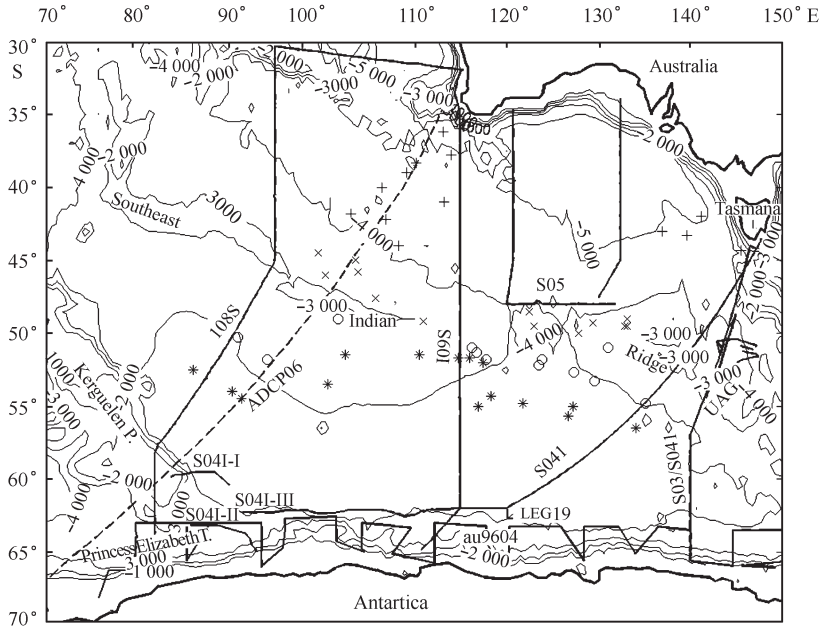

Fig. 1. Cruise tracks of ADCP velocity and hydrographic data used in this study and the positions of fronts in the southeast Indian Ocean obtained by Chinese scholars using the hydrographic data from historical Chinese National Antarctic Research Expedition (CHINARE) cruises and international cooperations. Each front has its own symbol: ＋STF; × SAF; ○ PF1; and ∗ PF2. Solid lines denote the cruise tracks from WOCE Global Data Version 3.0 and dashed line denotes the cruise track of the 14th CHINARE (1997~1998) cruise in the southeast Indian Ocean.

geostrophic current usually accompanies the fronts in the ACC. Therefore, the structure of baroclinic flow is one of the important properties of the fronts. Consequently, strong currents could be used to identify the fronts. Speed within the front is the measurement of the intensity of front and the orientation of current vector indicates the tangential direction of front path. In this study, we used ADCP and CTD data from six cruises in the southeast Indian Ocean from the WOCE global dataset and an ADCP section with synchronous upper potential temperature profiles obtained by the 14th CHINARE to examine the properties and spatial and temporal variations of currents within fronts.

2 Data

The ADCP and CTD data used in this study are from the WOCE Global Data Version 3.0 and the observations of the 14th CHINARE (1997~1998) in the southeast Indian Ocean. Cruises are listed in Table 1 and cruise tracks are shown in Fig.1. The WOCE ADCP data are hourly mean centered on the hour and linearly interpolated to a 10 m grid in vertical. Five out of seven cruises used in this study have synchronous CTD data. The raw ADCP data from the 14th CHINARE (1997~1998) have gone through a series of quality control procedures including original data check, time correction, data quality check, and calibration with vessel speed and position. Then the data with original resolution are averaged into hourly mean along the cruise track and then averaged or interpolated to a 20 m grid in vertical below 40 m in depth, which produces 26 levels of data. The synchronous temperature profiles measured by XBT and XCTD along the cruise track (the cooperation between the Polar Research Institute of China and the Lamont-Doherty Earth Observatory of Columbia University) are also used to assist the identification of fronts in the south-

Table 1. Cruises used in this study in the southeast Indian Ocean

Ship cruise	Date	Source	Abbreviation
09FA1094	Nov. to Dec. 1994	WOCE S05	S05
316N145-5	Dec. 1994 to Jan. 1995	WOCE I08S/I09S	I08S/I09S
09AR9404-1	Dec.1994 to Feb. 1995	WOCE S03/S04I	S03/S04I
Me1ville Cr.A9503	Mar. to Apr.1995	WOCE U S–Australia cooperative	UAC
09AR9604-1	Jan. to Mar.1996	WOCE au9604	au9604
320696-3	May to Jul.1996	WOCE S041	SO4I
CHINARE Cr14	Feb. to Mar.1998	Polar Research Institute of China	ADCP06

Notes: Abbreviations are used throughout the text.

east Indian Ocean. Data quality control can be found in Yuan et al. (2004).

Synchronous sea level anomaly (MSLA) data from the satellite altimeter are also used as references of in situ observations to examine the influence of eddies on the currents within fronts.

3 Strong currents and fronts in each section

3.1 WOCE Cruise S05

This cruise consists of two meridional sections (along 120°E from the Australian coast to 48°S and along 132°E from 48°S to the Australian coast) and one zonal section (along 48°S between those two meridional sections). The synchronous CTD observations are available (see Fig.1). By analysis of the three sections, a different results on the STF structure from the former study are observed, and it is a good example to examine the influence of the eddies on the currents within fronts.

The double STF structure exists apparently with maximal thermohaline gradients corresponding to the north STF between 36.5° and 37°S and south STF between 39.5° and 40.5°S at the depth less than 400 m in the vertical sections of potential temperature and salinity along 120°E (see Figs 2b and c). These two fronts are 3°of latitude apart , which conflicts with the frontal structure observed by BG96—the NSTF and SSTF merge into a single STF between 110° and 115° E. Corresponding to the SSTF, a strong flow with a speed exceeding 30 cm/s exists exactly at 40°S at the depth less than 150 m. However, the location of NSTF in the potential temperature and salinity sections does not coincide with the location of regional maximum speed in the ADCP section. The former is slightly south of the latter (see Fig. 2a). The reason is likely as follow. There is a rise pattern of the isopycnals below 400 m slightly north of the NSTF location (see Fig. 2d). The inverse inclinations of isopycnals below and above 400 m in the southern flank of the rise and the NSTF weaken the geostrophic current of the upper layer, while the geostrophic current in the northern flank of the rise is not weakened by the same mechanism. Consequently, the strong current occurs slightly north of the NSTF. In addition, surface temperature and salinity gradients near the STFs tend to compensate each other, resulting in a weak lateral density gradient in the surface layer. Therefore, detailed analyses are needed to identify the STF.

The SAF has intense lateral thermohaline gradients and extends to a deeper depth. The Subantarctic Surface Water subducts south of the SAF and spreads northward, which forms the minimum salinity layer—the Antarctic Intermediate Water. The Subantarctic Mode Water with relatively uniform density north of the SAF is captured in this transect. There are two flows exceeding 30 cm/s between 45° and 47° S (see Fig.2a), which are corresponding to the maximal thermohaline gradients between 45.5° and 46°S, and between 46.5° and 47°S respectively (see Figs.2b and c). The potential temperature and salinity change a little between these two high gradient zones. On the basis of

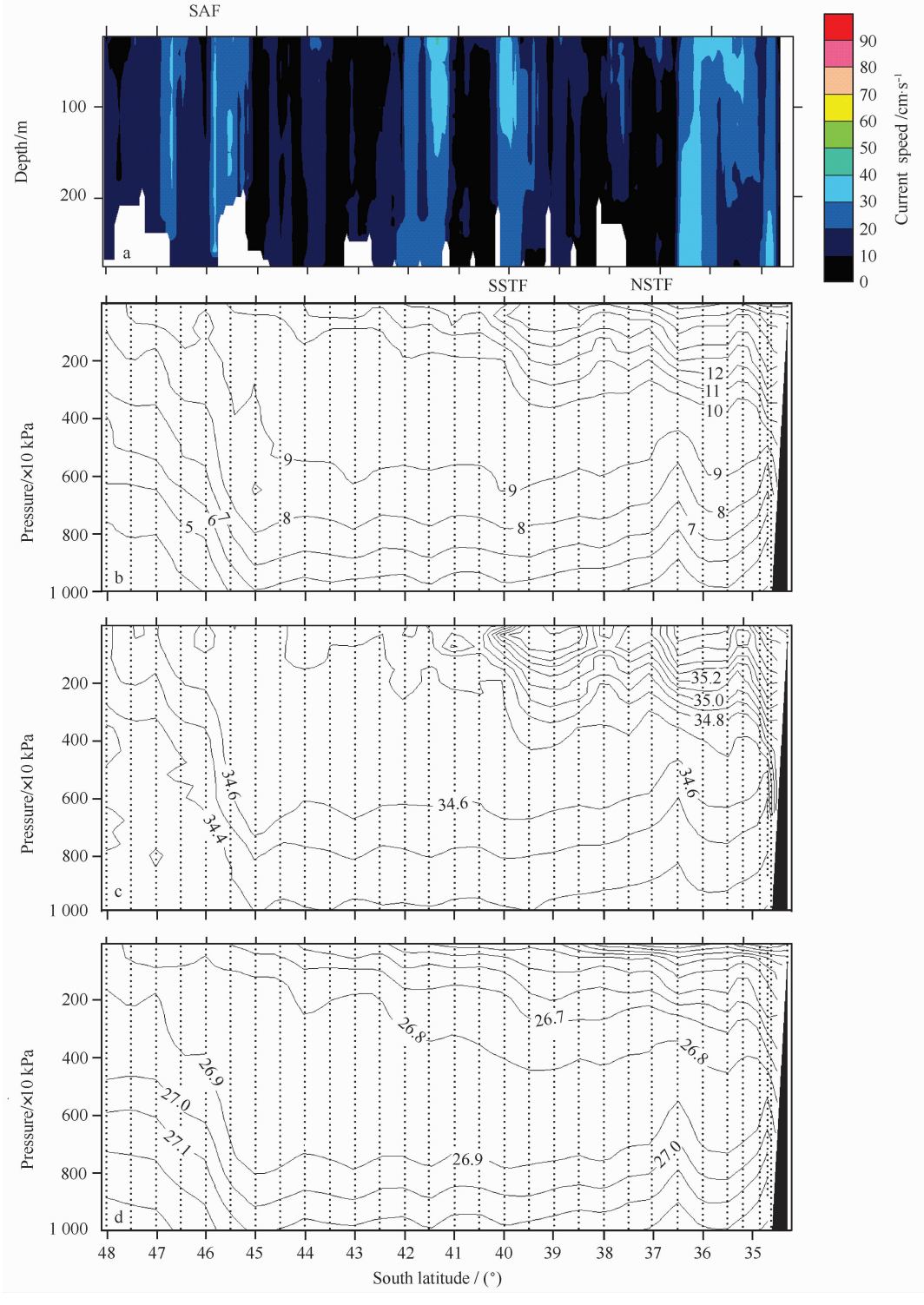

Fig. 2. Vertical sections of current speed(a), potential temperature (℃)(b), salinity(c) and potential density (kg·m^{-3}) (d) along 120°E in Cruise S05. The dotted lines are the location of each CTD cast.

intense thermohaline gradients extending to a great depth, we define this area as the location of the SAF. Two separate strong flows and weak thermohaline gradients between them mean that the strong current within the SAF splits into two branches. The north branch of SAF in this section may confluence the south branch along the dashed line showed in Fig.4 eddy in duced geostrophic current.

Two jets exist through the full depth measured by the ADCP in the zonal section along 48°S (see Fig.3a). One is between 122.5° and 123.8°E, and the other is between 125.6° and 126.5°E. The former, with the surface maximal current exceeding 100 cm/s, is much wider and stronger than the latter. There also exists a strong flow exceeding 30 cm/s between 120.5° and 121.2°E. These three jets all coincide with strong lateral thermohaline gradients (see Figs 3b and c). Considering the continuity of thermohaline isolines and potential vorticity conservation and based on the vectors of velocities measured by the ADCP at the depth of 20 m and contours of sea level anomaly on November 23(see Fig. 3d), we can conclude that the SAF is influenced by the out-of-phase double eddies located at 47.5°S, 122.7°E and 48.1°S, 125.3°E and runs across 48°S for three times. The current within the SAF can be strengthened by the geostrophic flow induced by the eddies. The maximal speeds are up to 47.9, 105.4 and 76.8 cm/s at 20 m depth respectively when the SAF runs across the section.

The only one strong current exceeding 40 cm/s exists near 46.8°S in the meridional section along 132°E, which coincides with the inclination of isopycnals produced by the eddy below 600 m in the thermohaline sections (not shown). Therefore, no strong surface current accompanies the STF that is located between 37° and 38°S.

3.2 WOCE Cruise I08S/I09S

This cruise includes two sections crossing the ACC from Frementle, Australia to the coast of Antarctica and return (see Fig. 1). These two sections ran across all the main fronts in the southeast Indian Ocean, which makes it possible to look into the correspondence between the strong currents and the main fronts.

Section I08S was occupied from 6 to 27 December heading south. The section starts southward along 95°E from approximate 30°S, turns southwestward after it reaches the Southeast Indian Ridge, crosses the south tip of Kerguelen Plateau and ends in the Princess Elizabeth Trough. According to the locations of strong currents and the thermohaline structure of the section (figure not shown), it can be concluded that the three jets locating at 42.5°, 48.8° and 51.4°S coincide with the SAF, the primary PF and the secondary PF, respectively. The double STF structure with ontense surface temperature gradient exists at 35° and 38°S. No strong current corresponds to those two fronts in the velocity field. A flow exceeding 20 cm/s at 63.5°S which is the strongest flow south of 58°S coincides with the intense salinity gradient within the SACCF. The location of this flow is in the Princess Elizabeth Trough, 0.5 of latitude south of the SACCF observed by Heywood et al.(1999) and near the southern limit of the SACCF proposed by OWN95. Contrasting to the SACCF observed by Heywood et al. (1999), the SACCF in this section can be identified more easily in salinity characteristics than in temperature characteristics.

Section I09S crossed the ACC northeastward from the slope of Antarctica at 110°E. After it reaches 62°S, 115°E, it turns northward along 115°E to Australia. Three jets are obvious in the velocity section. Referring to the thermohaline and density sections (figure not shown), these three jets are found to coincide with the locations of the secondary PF at 50.5 S, the primary PF at 48.6°S and the SAF at 46.0°S from south to north, respectively. The only one STF exists at 39.5°S without a corresponding strong current in the velocity section. The SACCF of this section also is located near the southern limit of the SACCF proposed by OWN95 and coincides with the current core at 62.2°S.

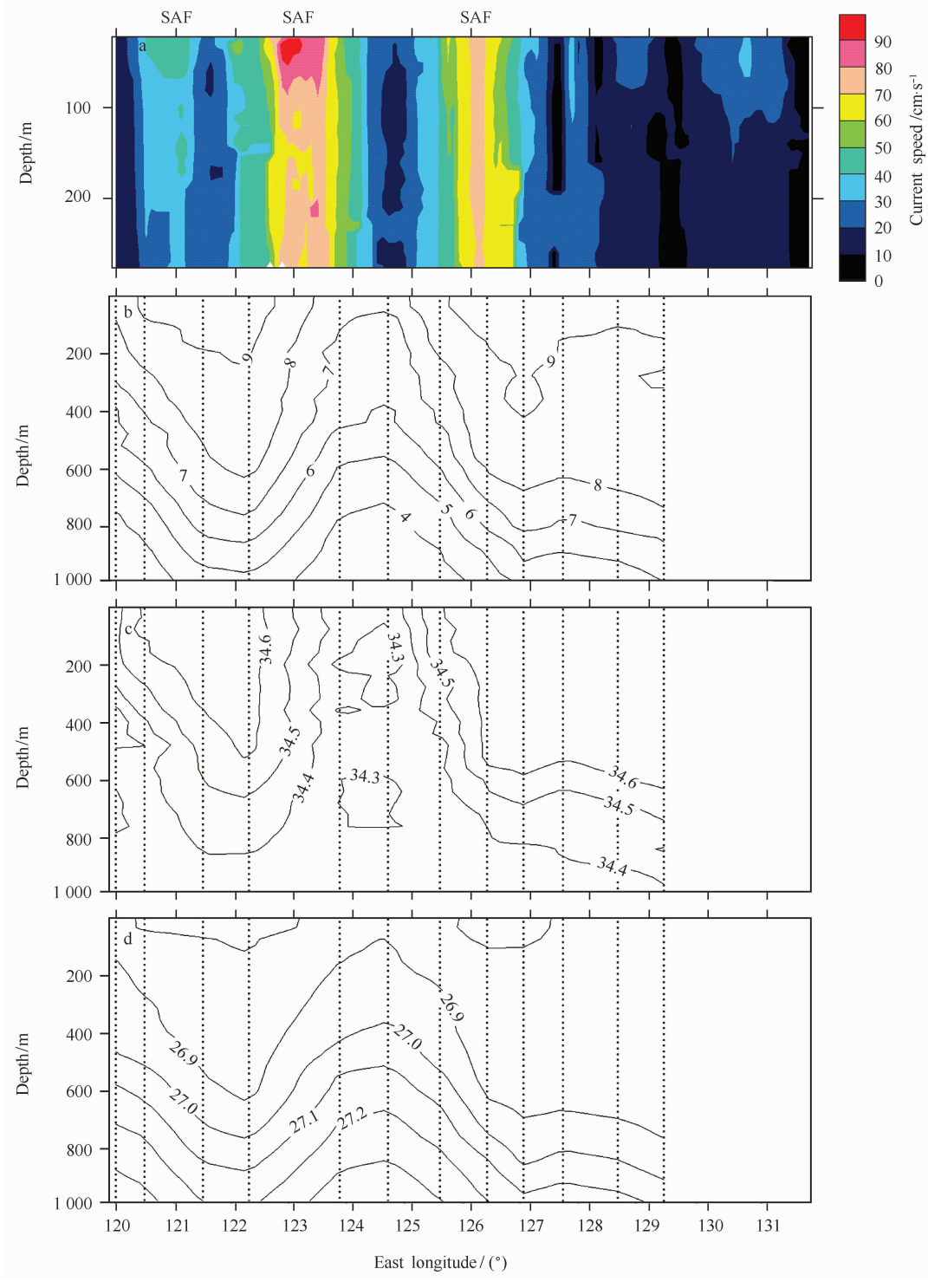

Fig. 3. Vertical sections of current speed (a), potential temperature (℃)(b), salinity(c) and potential density(kg·m^{-3})(d) along 48°S in Cruise S05. The dotted lines are the locations of CTD casts.

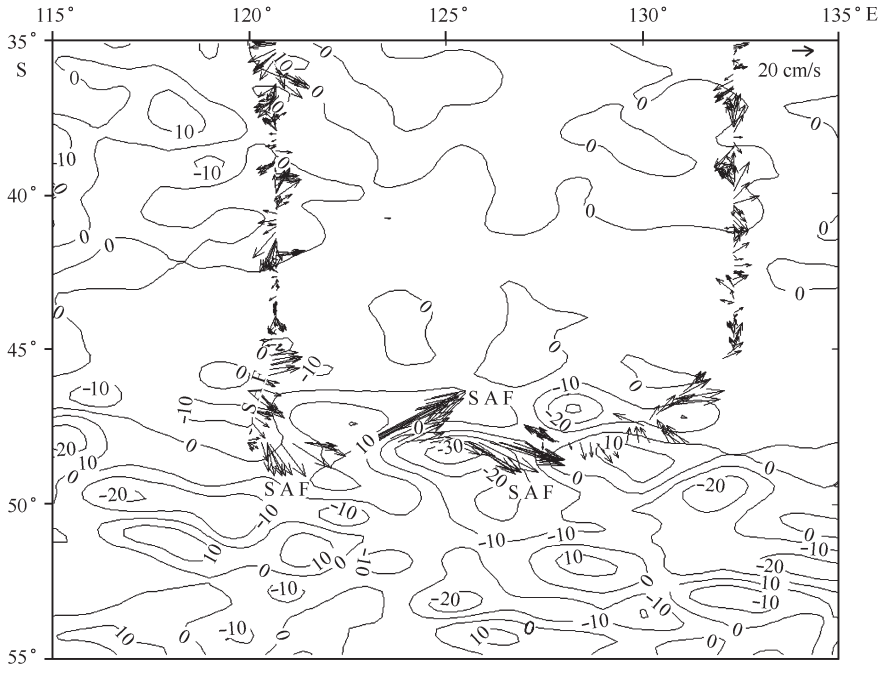

Fig. 4. Sea level anomalies and current vectors in the southeast Indian Ocean. The contours are sea level anomaly (cm) on 23 November 1994 derived from the measurement of altimeter and the vectors are current vectors of Cruise S05 at depth 20 m measured by ADCP.

3.3 WOCE Cruise S03/S04I and UAC

The section occupied by Cruise S03/S04I with ADCP and synchronous CTD observations extends northward from the slope of Antarctica along 140° E, turns northeastward at 56° S and ends at the southern tip of Tasmania Island in January 1995. It was repeated north of 55°S by Cruise UAC with only ADCP observations in April 1995 (see Fig.1). Comparison between these two sections shows the variation locations of the fronts.

Two jets exist through the full depth measured by the ADCP in the section of Cruise S03/S04I (figure not shown). The current cores of these two jets are located at 51.9° and 49.7° S corresponding to the primary PF and the SAF, respectively. No current core coincides with the secondary PF and the STF located at 53.6° and 45.5°S. Another current core at 63.8°S coincides with the southern limit of SACCF proposed by OWN95 and can be identified as the SACCF.

It is worth noting that the most powerful jet of Cruise UAC is located at 51°S with the speed exceeding 50 cm/s at the depth of 200 m and another jet is located at 51.3° S with the speed exceeding 40 cm/s at depth of 200 m (see Fig.5). Except for those two jets there are no other strong currents between 47° and 54.5°S. In the results of BG96, the positions of the SAF and PF along these longitudes are between 50° and 55°S, and are usually separated by 3° of latitude. It was also pointed out that they may join occasionally, although it is also likely that both fronts are still separable, and their confluence may be an artifact by wide station spacing. The two jets in this section should be the currents within the SAF and the primary PF, respectively. Although they are side by side, they can be identified as two fronts, which is benefited from the high spatial resolution of the ADCP data.

3.4 WOCE Cruise au9604

The circulation and water masses have been stud-

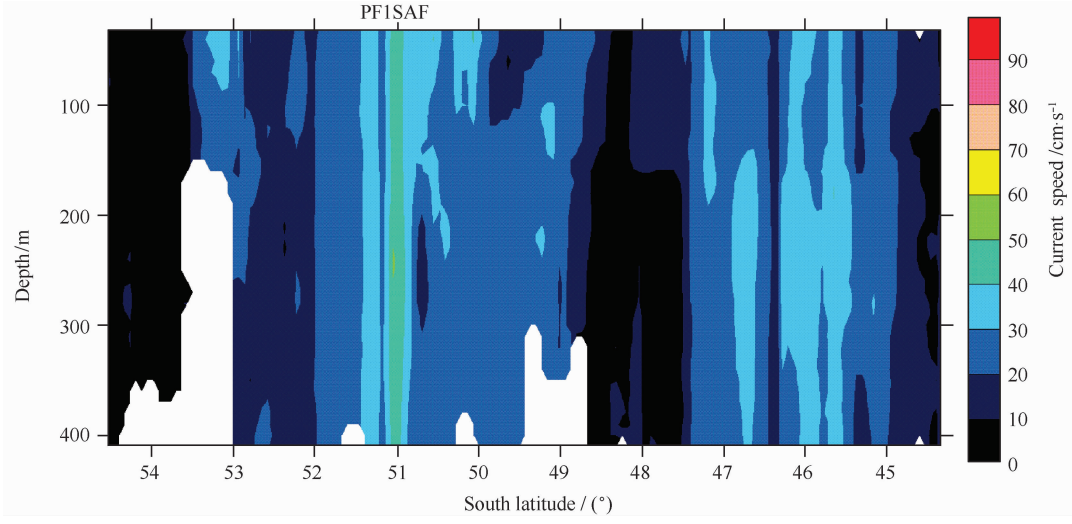

Fig. 5. Vertical section of velocity magnitude south of Tasmania Island measured from 8 to 14 April 1995 as part of Cruise UAC .

ied in detail by Bindoff et al. (2000) using CTD and ADCP data from this cruise. But the SACCF in this area has not been identified. In the present study we use the same data sets [current vectors were provided in the Fig. 9a of Bindoff et al. (2000)] and adopt the thermohaline criteria proposed by OWN95 to examine the properties of the SACCF in this area.

This cruise was undertaken from 30 January to 26 March 1996 along the east antarctic coast from 80° to 150°E (cruise track shown in Fig.1). The experiment consisted of eight North–South CTD sections and one irregularly spaced zonal section along approximately 63°S. The longitude of each meridional sections are listed in Table 2.

The irregularly spaced zonal section Leg 19 is labeled in Fig.1. The velocities are only available from WOCE Global Data Version 3.0 when ship was at station or moving with a speed of less than 0.35 m/s.

Not all the sections have signs of the SACCF. Only the sections that can be used to determine the path of the SACCF are shown below.

Section LEG1 along 80°E lies in the Princess Elizabeth Trough. The speed exceeds 30 cm/s at 64.5°S with a maximum in the proximity of 60 cm/s (Fig. 6b). The maximum speed is quite near the southern limit of the SACCF (64.3°S) determined by the salinity 34.73 isohaline below the depth of 800 m. Therefore it should be within the SACCF.

Along Section LEG19 (the quasi-zonal section along 63°S), the maximum of potential temperature and salinity both emerge in the west part of the section between Sections LEG1 and LEG4 (see Fig. 7). The maximum temperature (>2 ℃) occurs at the depth between 200 and 600 m and the maximum salinity (>34.73) occurs below the depth of 600 m, corresponding to the Upper Circumpolar Deep Water (UCDW) and Lower Circumpolar Deep Water (LCDW), respectively. This structure suggests that the southward intrusion of CDW in the west is stronger than that in the east between 80° and 94°E, so that the position of the southern limit of SACCF in the west should be at higher latitudes than that in the east. The SACCF can be identified between 84° and 86°E by its characteristic thermohaline isolines. Furthermore there exist relatively

Table 2. The longitude of each meridional section in the Cruise au9604

Section	LEG 1	LEG 4	LEG 7	LEG 9	LEG 11	LEG 13	LEG 16	LEG 18
East Longitude/(°)	80.0	93.6	104.4	112.3	120.3	128.4	139.8	150.0

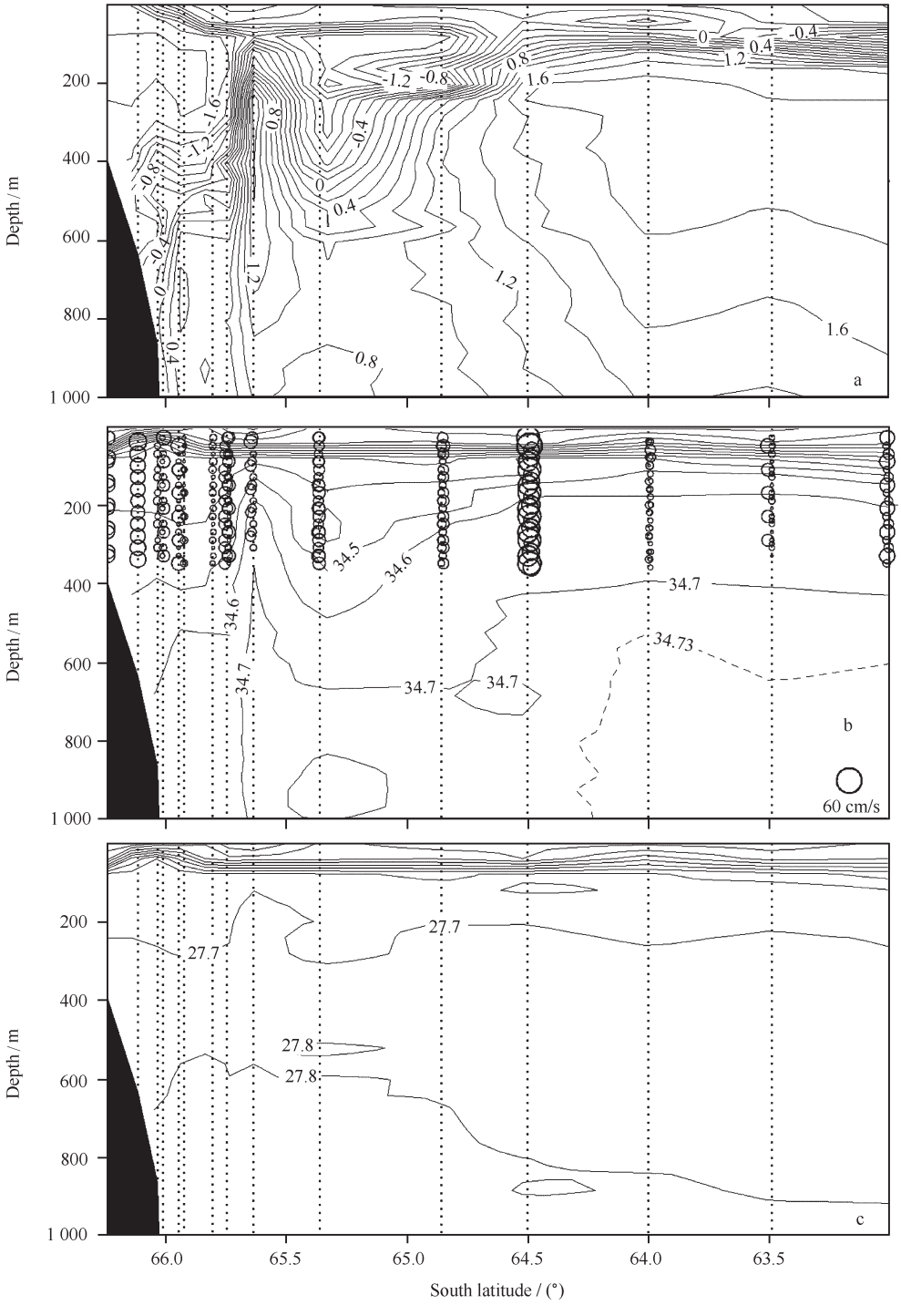

Fig. 6. Vertical sections of potential temperature(℃)(a), salinity(b) and potential density(kg/m^3)(c) of Section LEG1 along 80°E. The size of the circles indicates the speed measured by ADCP .

intense lateral temperature and density gradients below the depth of 150 m between these two longitudes. On the basis of the above information, we can confirm that the SACCF runs across the section between 84° and 86°E, although we cannot position the SACCF accurately from the current core because of the sparseness of ADCP sampling. The southward intrusion of UCDW centers at 82°E, which may mean that the SACCF turns southward after it crosses the meridian of 80°E, reaches its southernmost position at 82°E, and then turns

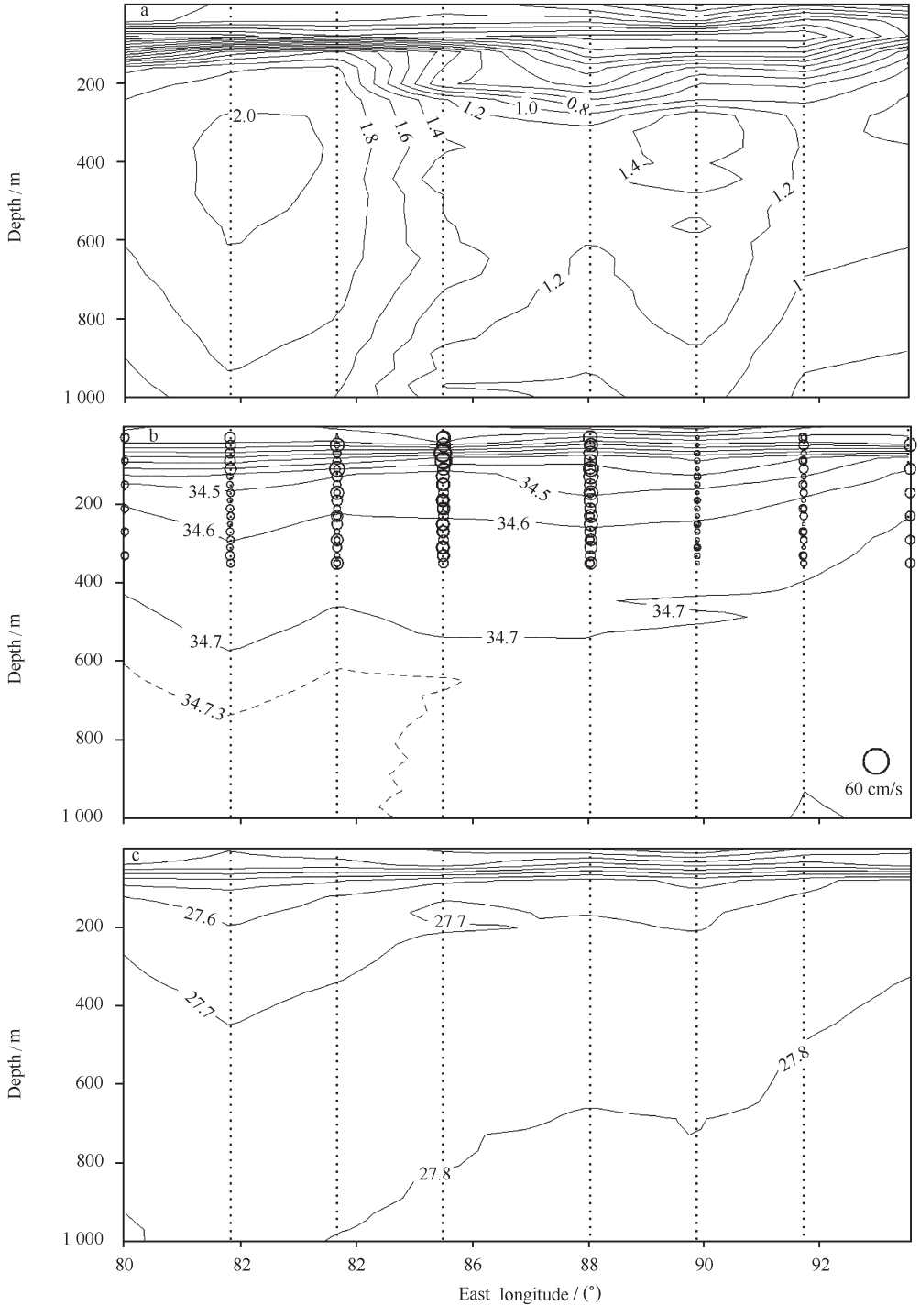

Fig. 7. As in Fig. 6, except for section of a part of the quasi-zonal Section LEG19 along about 63°S from LEG1 to LEG4 .

northward before it crosses the Section LEG19.

The thermohaline structures of the Section LEG11 (Fig.8) shows that the southern limit of SACCF is located north of the northern terminus of this section, and there is also no density gradient in the vertical section and no current core is measured in ACDP observations.

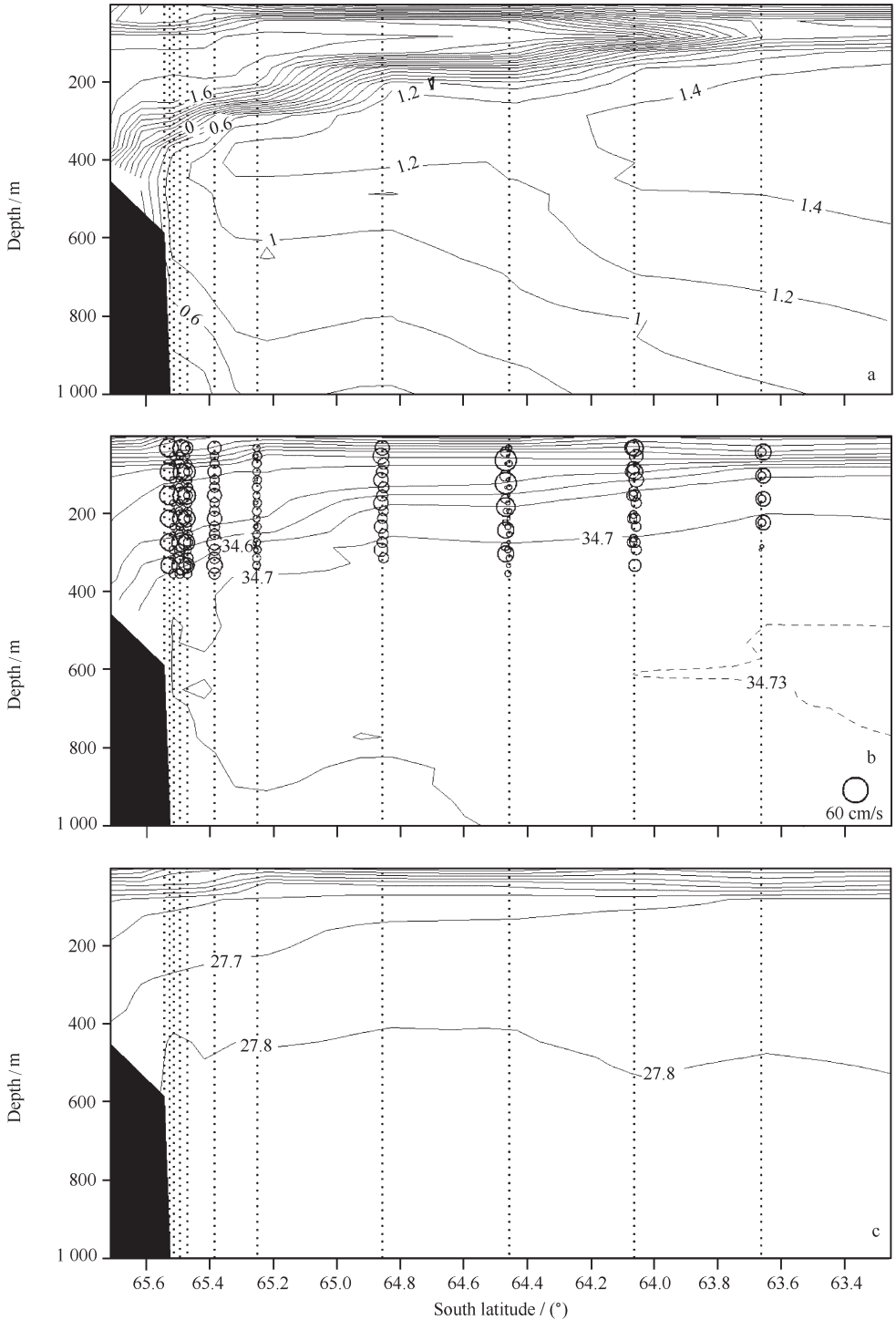

Fig. 8. As in Fig. 6, except for Section LEG11 along 120.3°E .

The most intense flow (exceeds 60 cm/s) along the Section LEG16 is located at 63.9 S (Fig. 9b), which coincides with the southern limit of the SACCF defined by the salinity isoline of 34.73 below the depth of 800 m and also corresponds to the density gradient below the depth of 100 m. Therefore the SACCF should cross the Section LEG19 between the Sections LEG11 and LEG16.

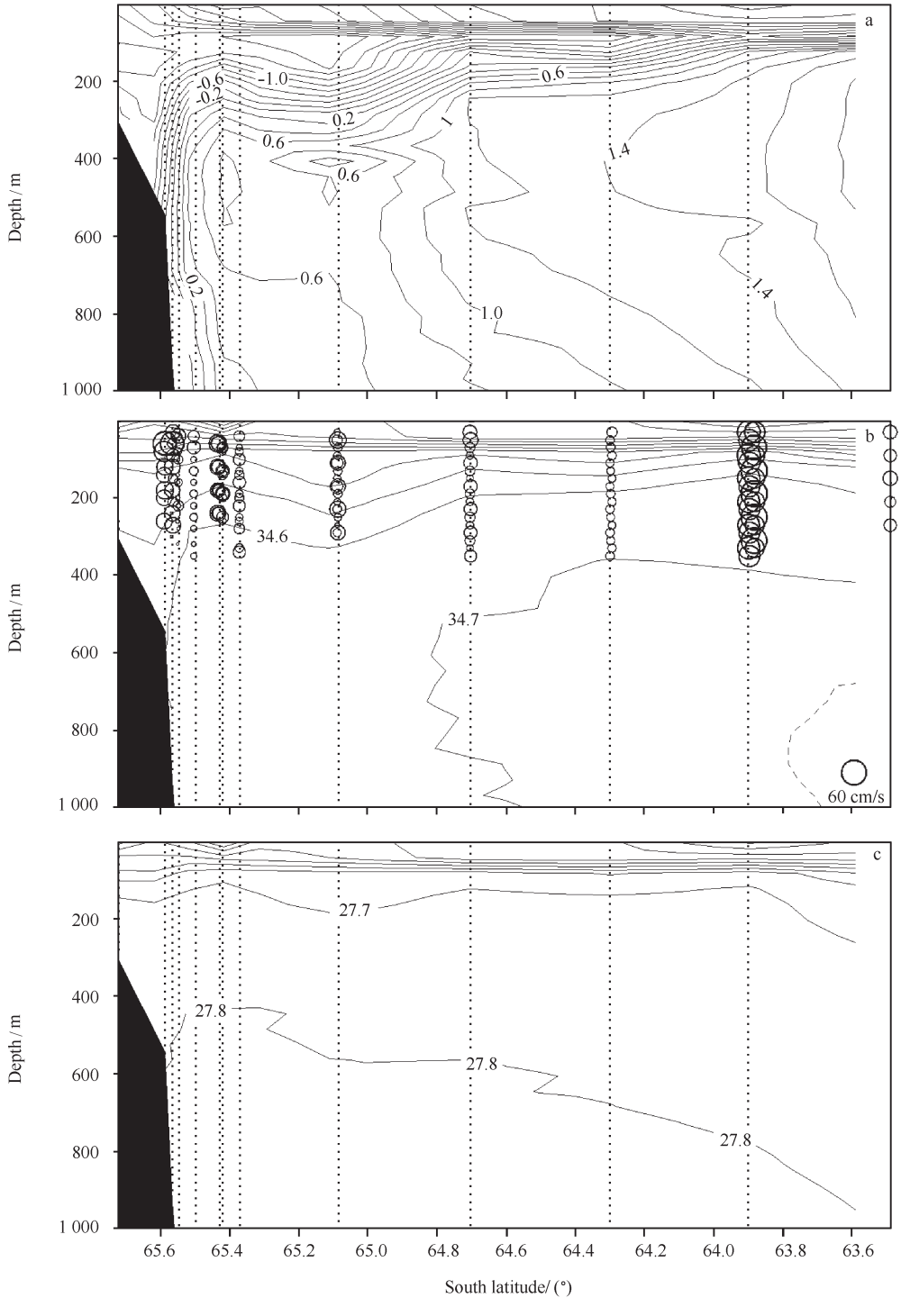

Fig. 9. As in Fig. 6, except for Section LEG16 along 139.8°E .

It can be judged that the southern limit of the SACCF crosses the Section LEG19 between 124° and 126°E from the 1.8 ℃ isotherm and the 34.73 salinity isoline in the thermohaline sections of Section LEG19 between Sections LEG11 and LEG16 (Fig.10). The southeastward flow exceeding 50 cm/s at 125.8°E and the high potential temperature and density gradients between 124° and 126°E further confirm that the SAC-

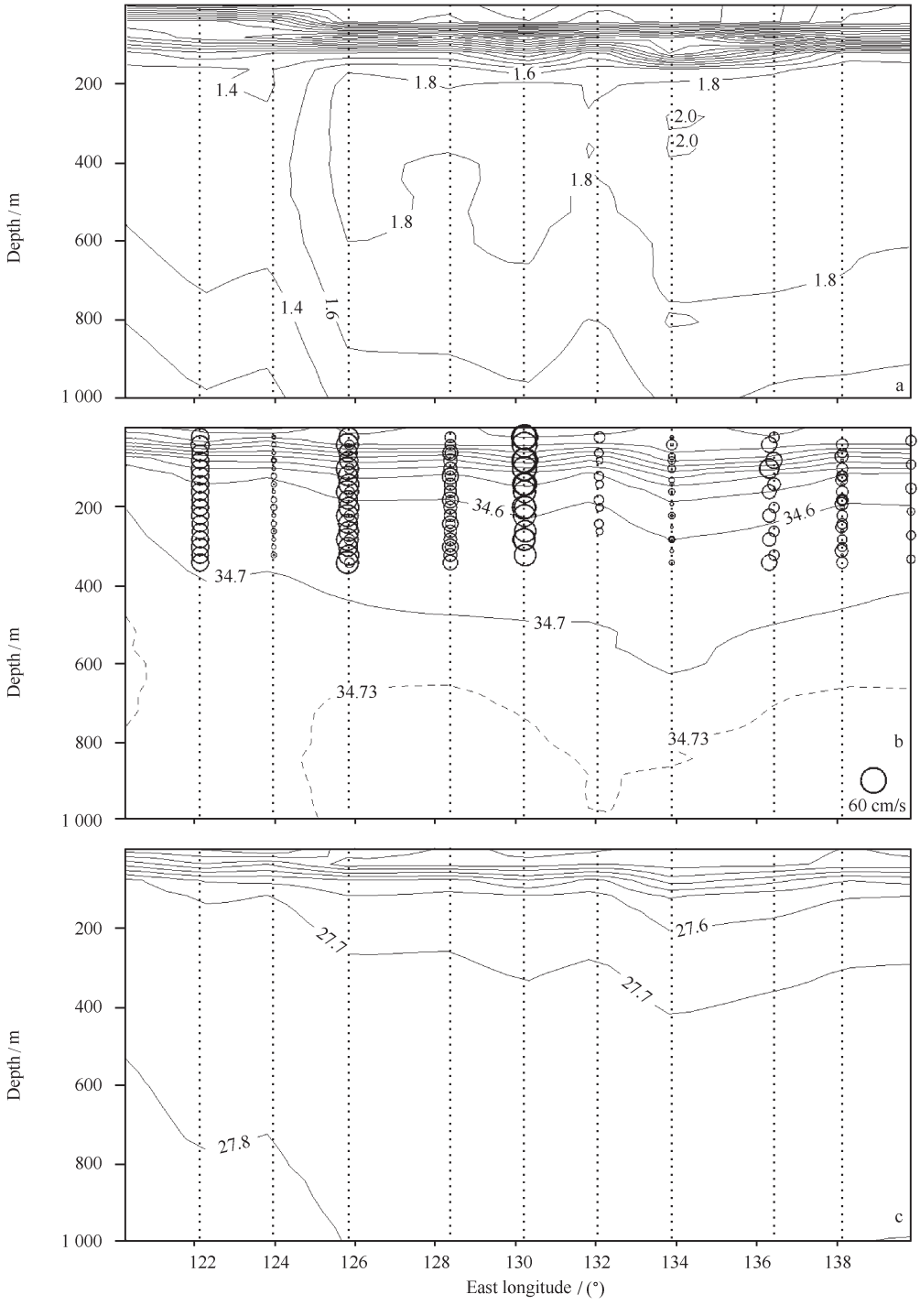

Fig. 10. As in Fig. 6, except for Section of a part of the quasi-zonal Section LEG19 along about 63°S from Sections LEG11 to LEG16 .

CF runs across Section LEG19 at this location.

According to the analysis above, the path of the SACCF in this cruise is proximately along the line in Fig.16.

3.5 WOCE Cruise S04I

This cruise was implemented in austral winter. It started from Cape Town, and navigated along 62°S between 20° and 124°E, then sailed northwest ending at Hobart (see Fig.1). In this study, we use the CTD and ADCP velocity data of the three sections between 80° and 124°E observed from 6 June to 3 July 1996 to examine the path of the SACCF along the cruise tracks in austral winter.

The first section investigated was in the area of 59.5°~60.5°S, 83.7°~90.0°E from 6 to 8 June 1996. The potential temperature and salinity distributions (see Figs 11c and d) show that the downwelling of cold water above 500 m and the upwelling of cold water below 500 m near 85.7° E separate the core of high-temperature and high-salinity CDW to the west and east with a high lateral temperature gradient between. According to the criteria of determining the southern limit of the SACCF by OWN95, the southern limit of the SACCF is located near 85°E and between 86° and 87°E in this section. On the basis of the speed section (see Fig. 11b) and velocity vectors at the depth 200 m (see Fig. 11a), we can conclude that the SACCF crosses this section northwestward and southward between 84.8° and 85.1° E, and at 86.8° E, respectively.

The second section was in the area of 63°~65.3°S, 84°~93° E from 14 to 19 June . The thermohaline properties of this section (see Figs 12a and b) are similar to that of the first section. The CDW is separated into two parts to the west and east by the downwelling at 86°E. The maximum potential temperature of the west part (>1.8 ℃) is warmer than that of the east part. The southern limit of the SACCF determined by the criteria of OWN95 is located near 85° E, so the SACCF should pass northward west of this position. Although the ADCP samples in this section are sparse, velocities exceeding 20 cm/s are measured at 84° and 85°E, just west of the southern limit of the SACCF, and should be the current core within the SACCF.

According to the thermohaline structures of these two sections above and their dissolved oxygen profiles (see Fig.13), the downwelling of the cold, less saline and oxygen-rich water column may result from the winter convection.

The third section is a quasi-zonal one investigated from 20 to 27 June along 62°S between 89.7° and 120° E. The southward intrusion of the CDW with several isolated cores below 200 m in the east part of the section is stronger than that in the west (see Figs 14c and d). On the basis of thermohaline criteria used in OWN95, the SACCF could cross this section a number of times. The weakest southward intrusion core is located at 98°E. A southward velocity exceeding 30 cm/s is observed below 110 m near 98.5° E (see Figs 14a and b). Because of the sparse sampling of ADCP data here, no clear northward returning flow associated with this southward intrusion is observed, so we cannot conclude that the flow at 98.5°E is within the SACCF. The second southward intrusion centers at 103.2°E. From the 34.73 salinity isoline below 800 m we can position the southern limit of the SACCF between 100°and 102.3°E, and near 107.4°E. The corresponding flows with the speed about 30 cm/s crossing the section southward at 102.3° E and northward at 107.4° E should be within the SACCF (see Figs 14a and b). The third southward intrusion is the most powerful one. The southern limit of the SACCF appears between 112° and 113.4°E. The southward flow exceeding 30 cm/s between 112° and 113° E should be the current within the SACCF (Figs 14a and b). These three positions of the SACCF all coincide with the lateral density gradients below 150 m (see Fig.14e).

From these three sections, the path of the SACCF in a cruise in austral winter is also similar to the path shown in Fig.16.

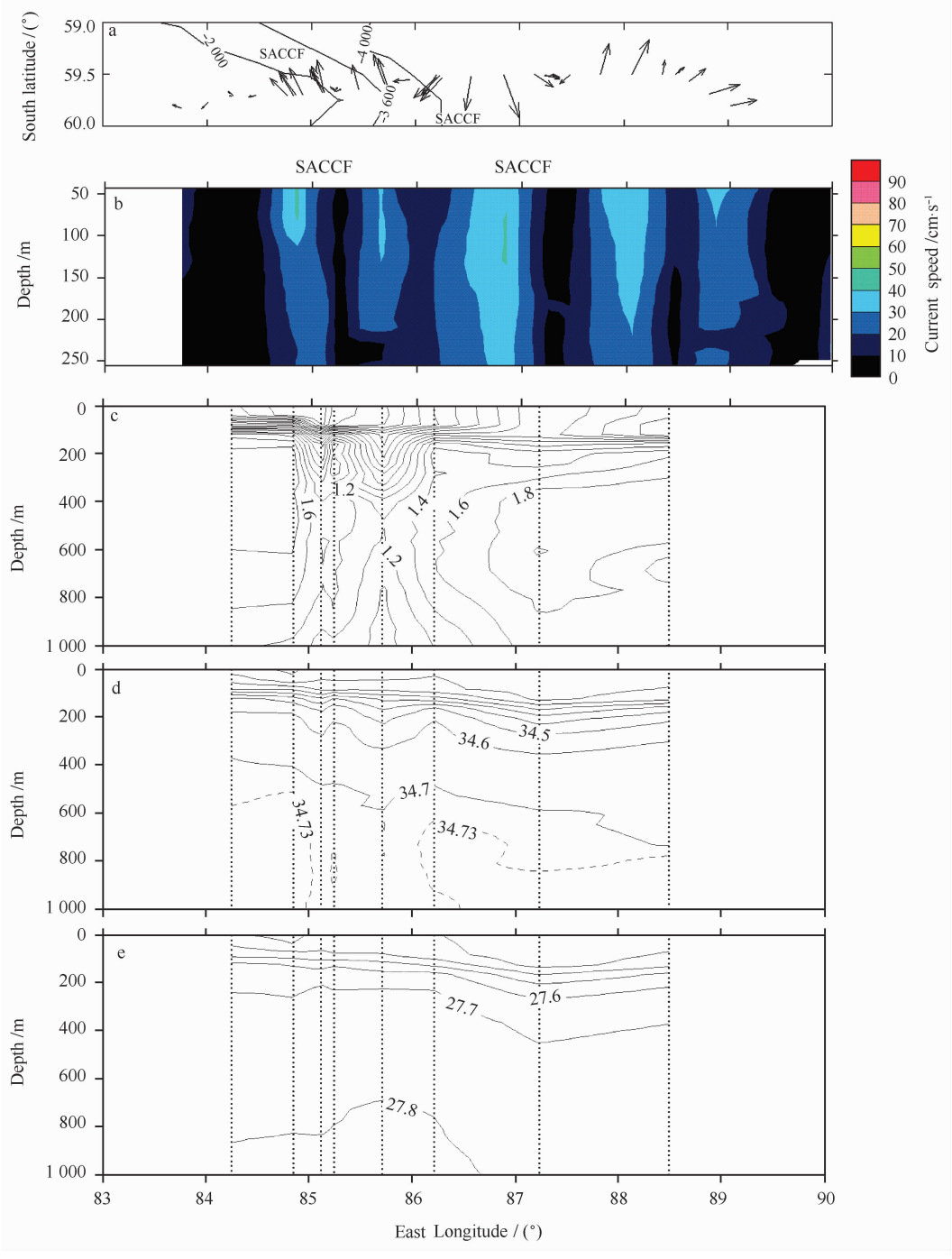

Fig. 11. Current vectors at depth 200 m (a), vertical sections of speed (b), potential temperature(℃)(c), salinity(d) and potential density(kg/m^3) (e) of the first part of Cruise S04I in the southeast Indian Ocean.

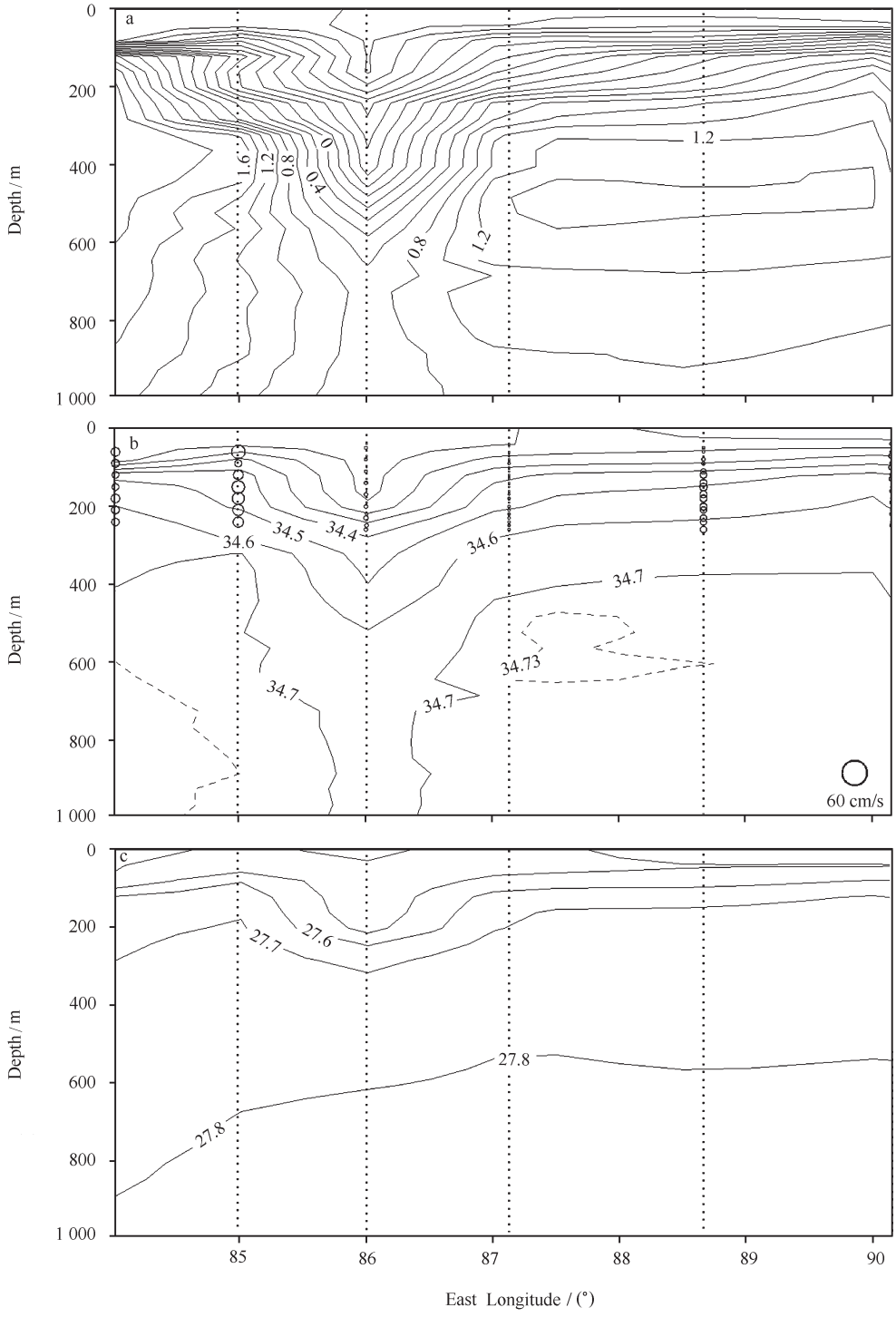

Fig.12. Potential temperature (℃)(a), salinity(b), potential density (kg/m^3)(c) of the second part of Cruise S04I in the southeast Indian Ocean. The size of the circles indicates the speed measured by ADCP.

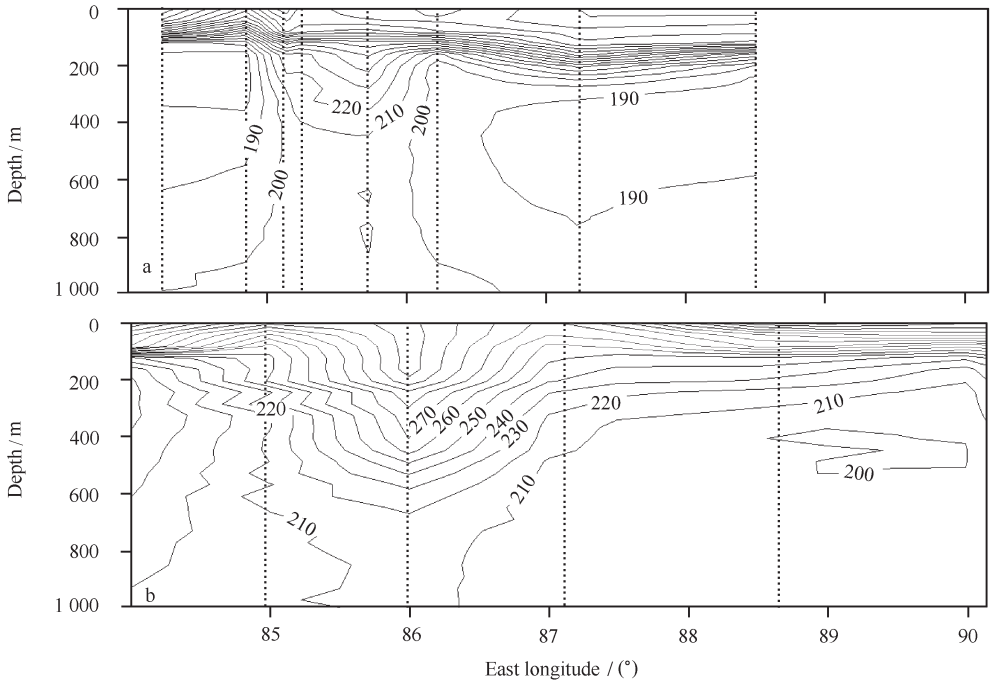

Fig. 13. Dissolved oxygen (μmol/kg) profiles of the first part (a) and second part (b) section Cruise S04I in the southeast Indian Ocean.

3.6 Fourteenth CHINARE ADCP06 Section

This ADCP section has synchronous temperature and salinity profiles measured by XBT and XCTD (see Fig.1). The XBT and XCTD stations are too sparse and unevenly distributed along the section to reveal the detailed thermohaline structures of this section, but can provide some clues to identifying the fronts corresponding to strong currents.

The maximum velocity of this section occurs between 50° and 51° S with the current core exceeding 130 cm/s (see Fig. 15a), which is right in the thermohaline range of the primary PF observed between 1998 and 2002 by Yuan et al. (2004). Station XCTD78 at 51°S, 96°E is right at the south edge of the jet. Its potential temperature profile shows that the temperature of full depth in the survey is warmer than 2 ℃ (see Fig. 15b), so this station must be located in north of the secondary PF. The temperature between 200 and 1 000 m does not vary much (<1 ℃), which also agrees with the property that isotherms near the front are vertical, therefore we can conclude that the primary PF is located at 50.3°S.

The next jet north of the primary PF is located at 45°S (see Fig.15a), and is right within the thermohaline range of the SAF observed by Yuan et al. (2004). The potential temperature profile of the Sta. XBT89 (39°S, 109.8°E) north of the jet and that of the Sta. XBT81 (47°S, 101.1°E) south of the jet (see Fig. 15b) have completely different properties. The temperature profile of the Sta. XBT89 has the typical structure of a subantarctic zone. The jet is the only one between these two profiles, suggesting that the jet is within the SAF.

The potential temperature of the minimum temperature layer of Sta. XBT71 (55° S, 90.5° E) is less than 2 ℃ (see Fig. 15b), so the secondary PF is located between 51°and 55°S. The two jets in these latitudes show a complicated structure, and it is difficult to determine which jet is corresponding to the secondary PF.

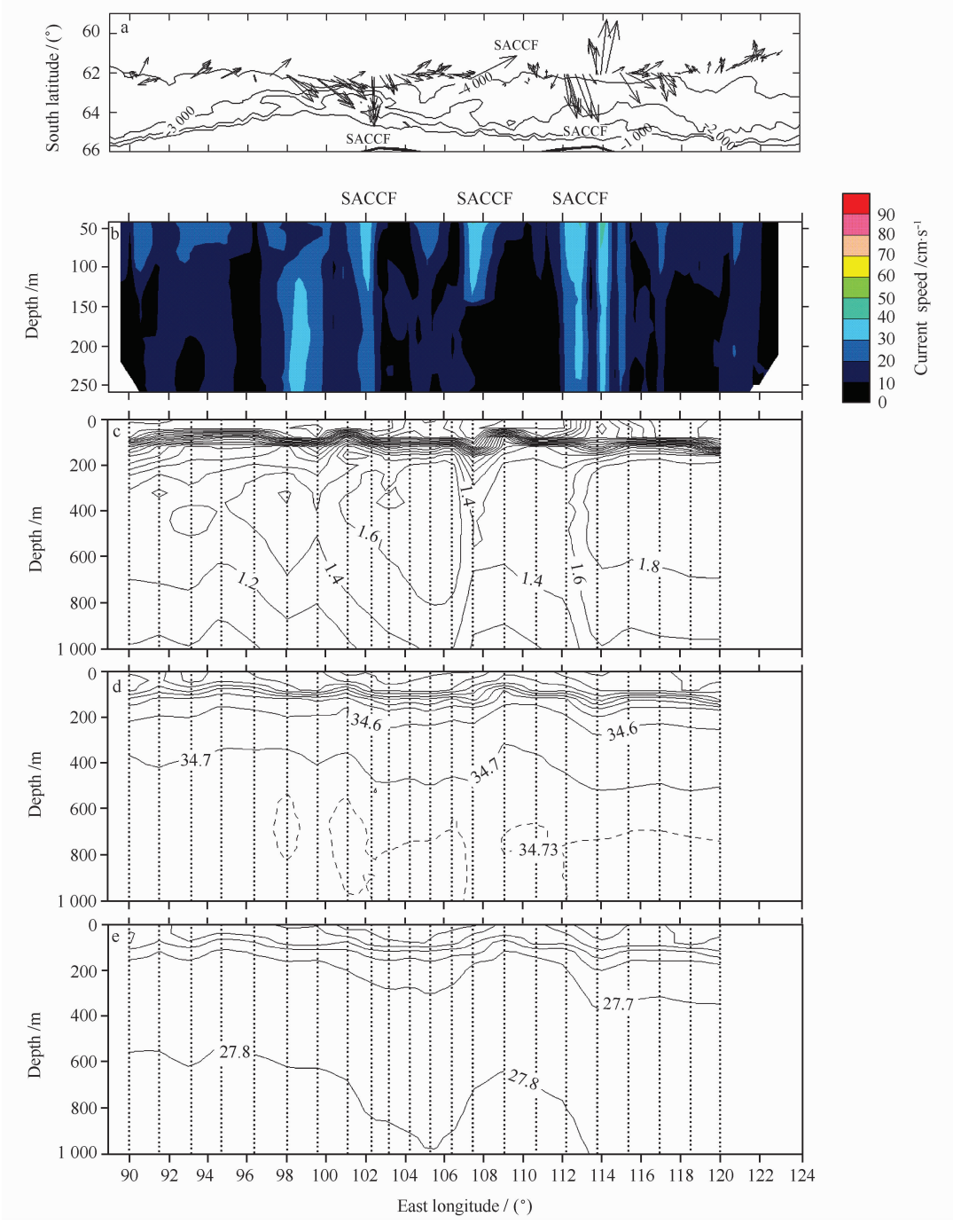

Fig .14. Current vectors at depth 140 m (a),vertical sections of speed(b), potential temperature (℃)(c), salinity(d) and potential density (kg/m^3) (e) of the third part of Cruise S04I in southeast Indian Ocean.

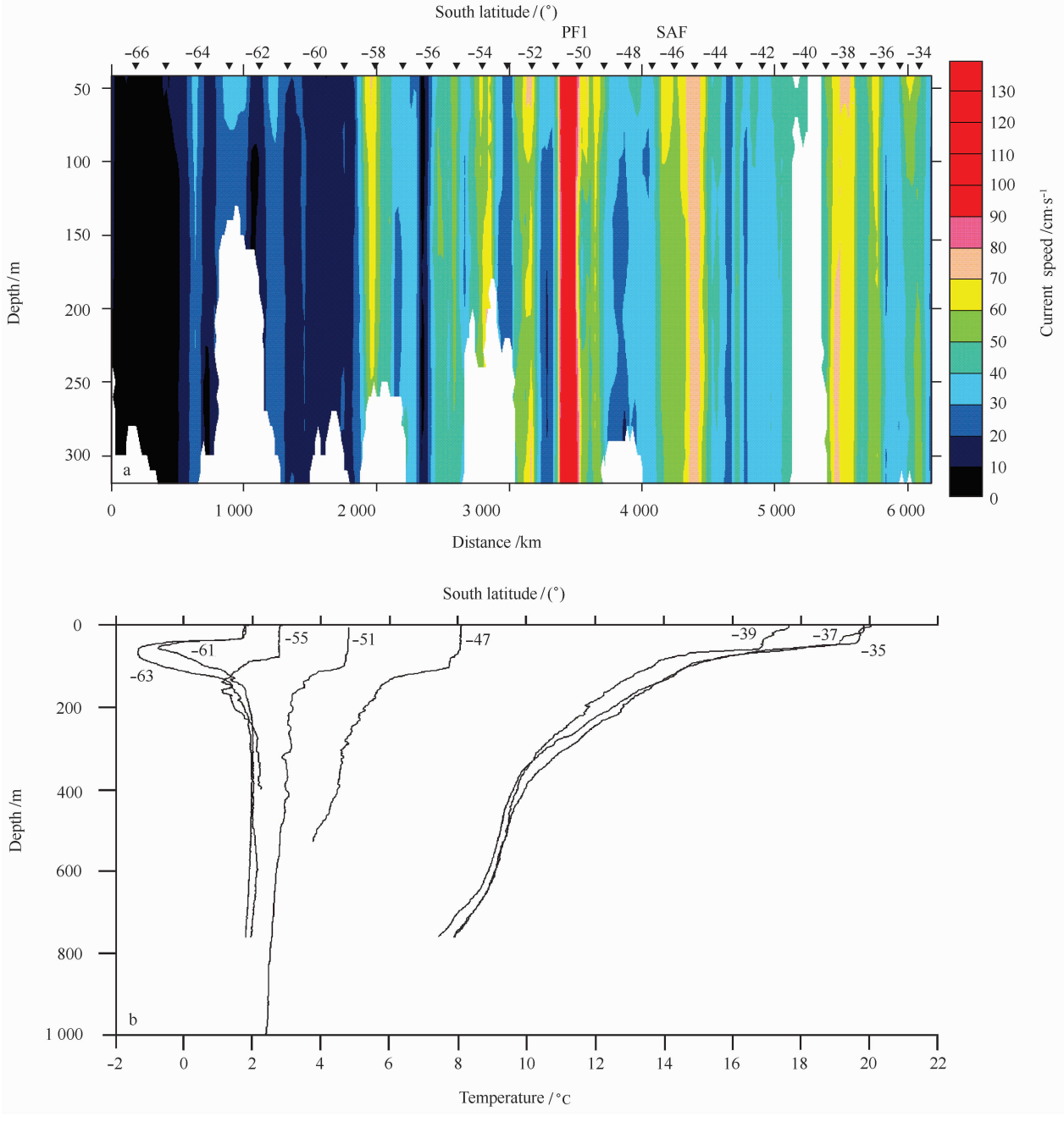

Fig. 15. Vertical section of the speed of Section 06 from the 14th CHINARE cruise (a) and the profiles of potential temperature measured by XBT and XCTD (b). The number above each profile is the latitude of each XBT or XCTD station.

4 Discussion

In the synoptic analysis of current and thermohaline data, we find that the SACCF in the southeast Indian Ocean always is located near the southern limit of the SACCF proposed by OWN95 where the potential temperature is warmer than 1.8 ℃ at the depth deeper than 500 m or where the salinity is greater than 34.73 at the depth deeper than 800 m. When the thermohaline data of Cruise au9604 were used to examine the water masses properties, Bindoff et al. (2000) pointed out that the temperature of the Circumpolar Deep Water (CDW) is warmer than 1.8 ℃ and the salinity is about 34.73 while the temperature of the Modified Circumpolar Deep Water (MCDW) is lower than 1.8 ℃ and salinity is less than 34.7. We also find that the SACCF always appears near the southern limit of the SACCF proposed by OWN95, which means that the SACCF exists right at the boundary of CDW and MCDW. Therefore the frontogenesis of the SACCF could result from the different thermohaline characteristics of the CDW and MCDW. The location of the SACCF is determined by the southward intrusion of the CDW.

Because the MCDW is the mixture of CDW and coastal water masses around the antarctic continent, the resulting thermohaline gradients between the CDW and MCDW are weak, but the density difference still exists (Figs 6c, 8c, 10c and 14e). Therefore, the SACCF is hardly defined by the strong thermohaline gradients. The CDW is the water column from subsurface to 3 000 m south of PF (Gordon, 1975). Baroclinic effect from the density difference between the MCDW and CDW integrated from the depth of 3 000 m to subsurface engenders a strong geostrophic current in the upper ocean. That is the reason why the current distribution can be used to identify the SACCF. Since this density gradient is relatively weak, the geostrophic current within the SACCF is less powerful than that of the SAF and the primary PF.

The SAF and the primary PF are both positioned at the locations with a strong thermohaline lateral gradient, then the local baroclinic effect results in strong geostrophic currents associated with these fronts. Therefore the locations, strength and orientation of these two fronts can be determined by the locations, speed and directions of velocity vectors of the jets. The secondary PF defined by the northern terminus of 2 ℃ isotherm does not always coincide with a jet, because it is not always associated with strong lateral thermohaline gradients. Therefore it is not reliable to identify this front by a jet. Although the STF is defined by the strong lateral thermohaline gradient, but the temperature and salinity gradients compensate each other within the front, resulting in weak density gradients. Therefore the STF cannot be identified by a jet.

The second part of Cruise S04I is quasi-zonal between 84° and 90° E and close to the part of LEG19 between the Sections LEG1 and LEG4 in Cruise au9604 (see Figs 7a and b). The common properties of these two sections are that two cores of southward intrusion of the CDW exist, and the one in the west is stronger than the one in the east. The difference between these two sections is that the CDW of this section is separated to the west and east parts by downwelling water in Cruise S04I, while there is no apparent downwelling water in the section of Cruise au9604, even with an upwelling phenomenon at 88°E in the potential temperature section. The east core of southward intrusion of the CDW in the second part of Cruise S04I is stronger and more westward than that in the section LEG 19 of Cruise au9604. The influence of the downwelling water on the density structure disappears below 600 m in Cruise S04I and the density distribution in both cruises is consistent below 600 m. Because these two sections were occupied in February and June respectively, the similar thermohaline properties mean that the thermohaline structure of the upper ocean in this area has little seasonal variation. The first part of Cruise S04I is 3° of latitude north of the second part and is implemented 6 d earlier. There is also downwelling water at 85.7°E. Because hydrograph-

ic data available in this area are rare in both austral summer and austral winter, whether the downwelling water near 86°E is the inherent characteristic in austral winter needs further investigation.

The underway ADCP data has advantages compared with the traditional thermohaline profile observations in identifying the main fronts in the Southern Ocean. First, velocity can give more information about fronts than thermohaline profiles. The position of the maximal speed is the core of fronts, and the magnitude of the maximal speed is a measurement of the intensity of fronts and the direction of velocity vector gives the extending orientation of fronts. Second, velocity sampling by ADCP has the advantage of higher spatial resolutions, which makes it possible to identify the spatial properties of fronts that are hard to be detected by the traditional thermohaline observations. Finally, the underway velocity sampling using ADCP is more convenient and more cost effective than the traditional hydrographic observations. It is superior that the operation can be done while navigating, especially in the rough in situ condition of the Southern Ocean. Therefore the underway velocity sampling by ADCP accompanied by some traditional hydrographic observations is an effective way to study the main fronts in the Southern Ocean.

5 Summary

(1) Double subtropical fronts are observed in the section along 120°E in Cruise S05—the distance between the NSTF and the SSTF is 3° of latitude, which conflicts with the frontal structure frequently observed before—the NSTF and SSTF merge into a single STF between 110° and 115°E. It likely reflects the variation of the STF.

(2) The SAF, influenced by the out-of-phase double eddies, runs across the section along 48° S in Cruise S05 three times. The surface current within the SAF is strengthened up to 105.4 cm/s by the geostrophic effect of those eddies. Furthermore eddies may cause the strong current within the SAF to split into two branches.

(3) The results of the historical observations in the southeast Indian Ocean (BG96), indicated that the SAF and the primary PF are the closest to each other between 140° and 145° E. Limited by the sampling density of hydrographic stations, sometimes it is difficult to identify whether these two fronts conflow to form a single front solely based on the thermohaline gradients. Benefited from the high resolution of ADCP data, we find an example that the SAF and primary PF do not conflow to form a single front with a separation distance of only 0.3° of latitude between two current cores in this area, although they cannot be identified separately in the low-resolution hydrographic data.

(4) Only minor differences exist between the paths of the SACCF observed in austral summer and winter, indicating that the path should be stable. The SACCF can be identified in ten sections through synthetic analyses of ADCP velocity, potential temperature and salinity. Except that the three sections of Cruise S04I were conducted in austral winter, the others were occupied in austral summer. If the seasonal variations are ignored, we can depict the mean path of the SACCF as shown in Fig.16. The SACCF turns northward along the east flank of the Kerguelen Plateau after it runs through the Princess Elizabeth Through and turns southward sharply north of 60°S. This path identified by synthetic analyses of ADCP velocity, potential temperature and salinity in our study agrees well with the SACCF found by the hydrographic data only in earlier studies (OWN95; Sparrow et al., 1996; Heywood et al., 1999; Shi et al., 2002).

(5) The present study is the first time that ADCP data have been used to identify fronts and indicates that the locations and orientations of the SAF, primary PF and SACCF in the ACC can be identified more precisely through the locations and orientations of jets coinciding with those fronts. The speeds listed in Table 3 below show that the SAF and the primary PF always coincide with jets (usually greater than 40 cm/s), while

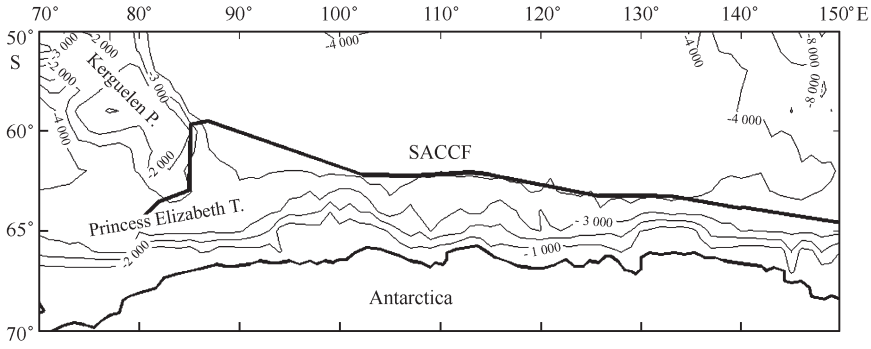

Fig.16. The path of the SACCF in the southeast Indian Ocean determined from ADCP data and hydrographic data used in this study.

Table 3. The current speed (cm/s) within each front measured at the depth of 200 m in each cruise

Cruise abbreviation	SAF	PF1	PF2	SACCF
S05	32.2 30.4 32.9 81.0 74.2			
I08S	45.5	44.8	52.4	26.1
I09S	75.9	65.0	58.6	29.2
S03/S04I	72.5	61.2	29.5	57.6
UAC	51.5	41.8		
au9604				42.3 53.8
S04I	50.4 41.9 67.8			24.2 37.1 29.2 33.5
ADCP06	79.0	133.3		
Mean	56.9	65.1	46.8	37.0

the secondary PF does not always coincide with a jet. The SACCF also coincides with a flow, but its speed is less than that of the SAF and the primary PF, and is usually between 20 and 40 cm/s. Therefore referring to the historical observations, the locations and orientations of the SAF, primary PF and SACCF can be identified solely by the locations and velocities of jets in the ACC.

Acknowledgments

We thank the WOCE Project Office and CLS Space Oceanography Division for supplying hydrographic data and altimeter products, respectively. The altimeter products were produced as part of the environment and climate EU ENACT project (EVK2-CT2001-00117). And we also thank Captain Yuan Shaohong and his crew of R/V Xuelong for the support of field operations.

This work was jointly supported by the National Natural Science Foundation of China undrer contract Nos 40376009, 40231013 and 49836010, and the Ministry of Science and Technology of China under con-

tract Nos 2003DIB4J135 and 2005DIB3J114, as well as the National Science Foundation of USA under contract No. OPP0230284.

References

Belkin I M, Gordon A L. 1996. Southern Ocean fronts from the Greenwich meridian to Tasmania. J Geophys Res,101: 3 675~3 696

Bindoff N L, Rosenberg M A, Warner M J.2000. On the circulation and water masses over the Antarctic continental slope and rise between 80° and 150°E. Deep-Sea Res(Part II), 47: 2 299~2 326

Emery W J. 1977. Antarctic polar frontal zone from Australia to the Drake Passage. J Phys Oceanogr, 7:811~822

Fandry C, Pillsbury R D. 1979. On the estimation of absolute geostrophic volume transport applied to the AACC. J Phys Oceanogr, 9:449~455

Gao Guoping, Liu Qi, Shi Maochong. 1995. Position of the southern polar front in the Indian Ocean and separation of the surface submergence water in the Antarctica. Journal of Ocean University of Qingdao, 25 (Sup): 424~431

Gao Guoping, Han Shuzong, Dong Zhaopian, et al. 2003. Structure and variability of fronts in the South Indian Ocean along sections from Zhongshan Station to Fremantle. Acta Oceanologica Sinica (in Chinese), 25(6): 9~19

Gordon A L.1971. Antarctic polar front zone. In: Antarctic Oceanology. I, Antarct Res Ser, v 15, 205~221, Washington, D. C: AGU

Gordon A L. 1975. An antarctic oceanographic section along 170° E. Deep-Sea Res, 22: 357~377

Hamon B. V. 1965. The East Australia current 1960—1964. Deep-Sea Res, 12, 899~921

Heywood K J, Sparrow M D, Brown J, et al. 1999. Frontal structure and Antarctic Bottom Water flow through the Princess Elizabeth Trough, Antarctica. Deep-Sea Res(Part I), 46:1 181~1 200

Miao Yutian, Yu Honghua, Xu Janping, et al.1995. The temperature distribution and the front characteristics along sections of southwest Prydz Bay. Journal of Ocean University of Qingdao, 25(Sup): 383~393

Moore J K, Abbott M R, Richman J G. 1999. Location and dynamics of the Antarctic Polar Front from satellite sea surface temperature data. J Geophys Res, 104(C2): 3 059~3 073

Nowlin W D Jr, Clifford M A. 1982. The kinematic and thermohaline zonation of the AACC at Drake Passage. J Mar Res, 40(Sup): 481~507

Orsi A H, Whitworth T III, Nowlin W D Jr. 1995. On the meridional extent and fronts of the Antarctic Circumpolar Current. Deep-Sea Res (Part I), 42:641~673

Pu Shuzhen, Hu Xiaomin, Dong Zhaoqian, et al. 2002. Circumpolar deep water and Antarctic Bottom Water and their characteristics around Prydz Bay, Antarctica. Acta Oceanologica Sinica(in Chinese), 24(3): 1~8

Shi Jiuxin, Le Kentang, Choi B H. 2002. The pattern and seasonal variation of the circulation in the region of the Kerguelen Plateau. Acta Oceanologica Sinica (in Chinese), 24(4): 11~22

Shi Maochong, Miao Yutian, Yu Honghua, et al. 1995. Characteristics and variation of summer frontal zone along 110° E in South Indian Ocean. Journal of Ocean University of Qingdao, 25(Sup): 394~405

Sparrow M D, Heywood K J, Brown J. et al. 1996. Current structure of the south Indian Ocean. J Geophys Res, 101: 6 377~6 391

Su Yufen, Dong Zhaoqian. 1984. The fronts and hydrographic characteristics in the Southern Indian Ocean during summer. Collecting Papers of Antarctic Researc, n2.Beijing:China Ocean Press, 25~40

Sun C, Watts D R. 2002. A view of ACC fronts in streamfunction space. Deep Sea Res.(Part I), 49:1 141~1 164

Yuan X, Martinson D G, Dong Z. 2004. Upper ocean thermohaline structure and its temporal variability in the southeast Indian Ocean. Deep-Sea Res.,(Part I), 51:333~347